Electronic Supplementary Information

In-situ nanoarchitecturing of conjugated polyamide network-derived carbon cathodes toward high energy-power Zn-ion capacitors

Xunwen Zheng,[a‡] Ling Miao,[a‡] Ziyang Song,[a] Wenyan Du,[a] Dazhang Zhu,[a] Yaokang Lv,[c] Liangchun Li,[a] Lihua Gan,[a,*] Mingxian Liu[a, b,*]

[a]*Shanghai Key Lab of Chemical Assessment and Sustainability, School of Chemical Science and Engineering, Tongji University, Shanghai 200092, P. R. China.*

[b]*College of Chemistry and Molecular Engineering, Zhengzhou University, Zhengzhou 450001, P. R. China.*

[c]*College of Chemical Engineering, Zhejiang University of Technology, Hangzhou 310014, P. R. China.*

***Corresponding Authors**

E-mail: ganlh@tongji.edu.cn (Lihua Gan), liumx@tongji.edu.cn (Mingxian Liu).

‡ These authors contributed equally to this work.

Characterization

The morphological and elemental images are acquired using scanning electron microscopy (SEM, Hitachi S-4800) equipped with an X-ray energy dispersive spectroscopy (EDS) instrument. Fourier transformed infrared spectra (FT-IR) are conducted using a Thermo Nicolet NEXUS spectrometer. X-ray diffraction (XRD) patterns are obtained on a D8 Advance X-ray diffractometer (Cu Ka radiation source λ= 0.154 nm). Raman spectra are analyzed using a Renishaw Invia (λ_{exc} = 514 nm). The nitrogen adsorption/desorption isotherms are analyzed on a Micromeritics ASAP 2460 apparatus at −196 °C. The surface area is obtained by Braunauer−Emmett−Teller method. The pore size distribution is evaluated by the nonlocal density functional theory model. The surface functionality is acquired by an X-ray photoelectron spectrometer (XPS, AXIS Ultra DLD). Ultraviolet visible near infrared (UV-vis-NIR) spectra are conducted by an Agilent Carry 5000 spectrometer.

Electrochemical Measurements

The working electrode is prepared by mixing the prepared carbon with carbon black and polytetrafluoroethylene binder with a weight ratio of 8:1:1 in ethanol. After drying at 80 °C overnight, the mixture is pressed on the stainless-steel mesh (mass loading of electroactive materials: ~10 mg cm^{-2}) under 20 MPa and then dried overnight at 60 °C. Zn-ion hybrid capacitors are assembled with the working electrodes as the cathode, Zn foil as the anode, 3 mol L^{-1} aqueous $Zn(CF_3SO_3)_2$ solution as the electrolyte, and a glassy fibrous as the separator.

The cyclic voltammetry (CV) and electrochemical impedance spectroscopy (EIS) measurements are performed on a CHI660E electrochemical workstation. Galvanostatic charge/discharge (GCD) measurements are conducted on the CT3001A battery test system. All devices are tested within the

potential range from 0 to 1.8 V. The gravimetric capacitance (C_m, mA h g^{-1}), energy density E (W h kg^{-1}), and power density P (kW kg^{-1}) of the devices are obtained from the following equations.

$$C_m = \frac{I \times \Delta t}{m} \tag{2}$$

$$E = C_m \times \Delta V \tag{3}$$

$$P = \frac{C_m \times \Delta V}{1000 \times \Delta t} \tag{4}$$

where I is the current density, Δt is the discharging time, and m is the mass of active material, ΔV is the voltage window.

The ion diffusion coefficient (D, cm^2 s^{-1}) is calculated according to the following equation.

$$D = \frac{R^2 T^2}{2A^2 C^2 F^4 n^4 \sigma^2} \tag{5}$$

where R (8.314 J mol^{-1} K^{-1}), T (293.15 K), A (m^2 g^{-1}), C (mol L^{-1}), F (96485 C mol^{-1}), n, σ (Ω $s^{-0.5}$) is gas constant, Kelvin temperature, the surface area of electrodes, molar concentration of electrolyte, Faraday constant, electron transfer numbers per molecule during electron reaction, and diffusive resistance, respectively.

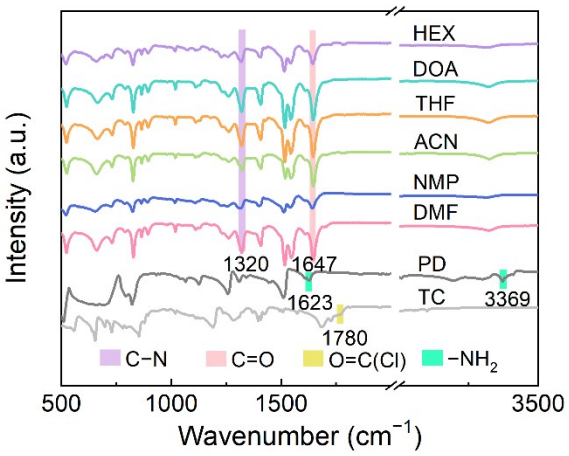

Fig. S1 FT-IR spectra of monomers and polyamide precursors prepared by diverse solvents.

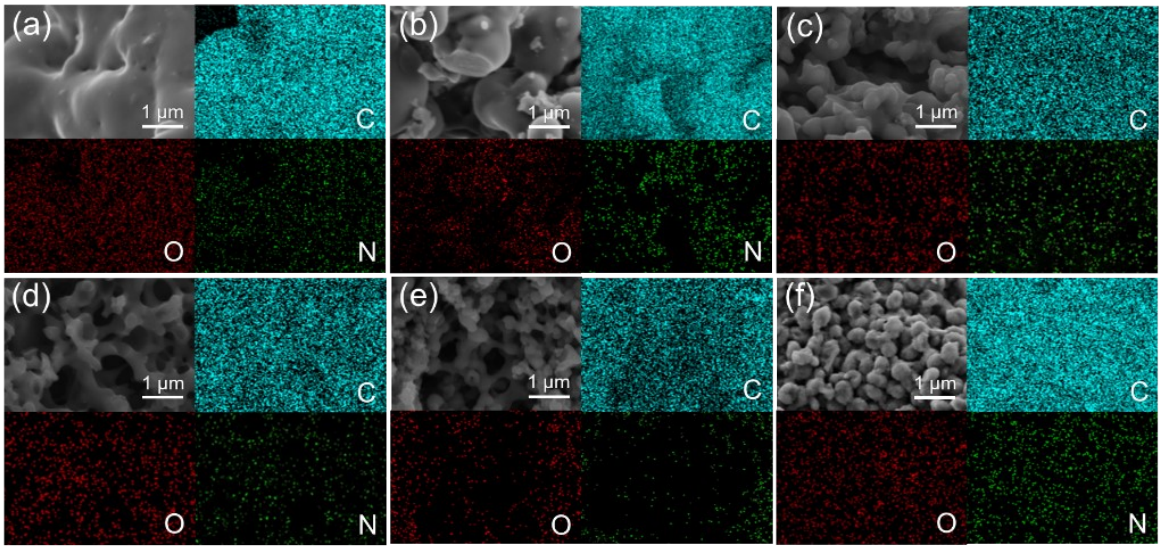

Fig. S2 SEM images and the EDS mappings of (a) C_{HEX}, (b) C_{DOA}, (c) C_{THF}, (d) C_{ACN}, (e) C_{NMP}, and (f) C_{DMF}.

Hansen Solubility Parameters Experiments

Hansen solubility parameters (HSPs) are estimated by a series of dispersibility experiments according to the literature.[1-3] Specifically, polyamide is added into ten common solvents with known HSPs and ultrasonicated for 1 h. Hereafter, the obtained dispersions are stabilized for one day, and the concentrations of the polyamide in the supernatant of the dispersions are then estimated by measuring the UV-vis absorption spectrum at 560 nm. Based on the concentration of the polyamide calculated by the Beer-Lambert-Bouguer law and observation of the swollen state and the sedimentation of polyamide in the suspension, the solvents with high reactivity to precursors own closer HSPs of the material than the solvents with low reactivity. Therefore, the three HSPs of polyamide are calculated by developing a three-dimensional model based on Hansen theory, where the ball center is the HSPs of the studied materials and the radius value (R_o) presented the maximum difference in affinity allowed for a high interaction between solvent and material. Based on this method, the HSPs of polyamide are experimentally determined in Fig. 1h and the HSPs values of the polymer are estimated to be 25.8 $MPa^{0.5}$ (Table S1). The distance between the solvent and the material (Ra) can be evaluated with Equation (1).

$$R_a^2 = 4(\delta_{D,\,solu} - \delta_{D,\,solv})^2 + (\delta_{P,\,solu} - \delta_{P,\,solv})^2 + (\delta_{H,\,solu} - \delta_{H,\,solv})^2 \quad (1)$$

where δ_D, $\delta_{P,}$ and δ_H refer to the dispersion, polar, and hydrogen parameters, respectively. The subscripts are “solu” for the studied solute material and “solv” for solvents.

Table S1 Summary of HSPs between diverse solvents and the precursor.

	Solvent/Precursor	δ_T	δ_D	δ_P	δ_H	Absorbance[a]	Polymerisation[b]	R_a	RED	Data fit
1	Hexane	14.9	14.9	0.0	0.0	0.007	√	19.6	1.7	1
2	1,4-Dioxane	20.5	19.0	1.8	7.4	0.155	√	13.7	1.2	
3	Tetrahydrofuran	19.5	16.8	5.7	8.0	1.797	√	9.7	0.8	
4	Acetonitrile	24.4	15.3	18.0	6.1	2.575	√	8.5	0.7	
5	*N*-methyl pyrrolidone	23.0	18.0	12.3	7.2	2.265	√	5.4	0.5	
6	Dimethyl formamide	24.9	17.4	13.7	11.3	2.702	√	1.2	0.1	
7	Isopropanol	24.0	17.6	6.1	15.1	3.043	×	–	–	
8	Dimethyl sulfoxide	26.7	18.4	16.4	10.2	2.431	×	–	–	
9	Propylene carbonate	27.2	20.0	18.0	4.1	3.048	×	–	–	
10	Methanol	29.6	15.1	12.3	22.3	1.966	×	–	–	
	Polyamide	25.8	17.6	14.3	12.2	–	–	–	–	–

[a]Measured absorbance at 560 nm.

[b]The first six solvents are selected as reaction media because the polymerization occurs in these systems.

Table S2 Surface areas (S_{BET}), micropore surface areas (S_{micro}), total pore volumes (V_{tol}), and chemical compositions of C_X.

Sample	S_{BET} ($m^2\ g^{-1}$)	S_{micro} ($m^2\ g^{-1}$)	V_{tol} ($cm^3\ g^{-1}$)	O (wt.%)	N (wt.%)
C_{HEX}	942	798	0.54	6.61	3.88
C_{DOA}	1035	881	0.61	6.70	4.35
C_{THF}	1110	982	0.62	7.58	4.85
C_{ACN}	1223	1192	0.62	9.14	5.76
C_{NMP}	1486	1466	0.63	9.04	6.12
C_{DMF}	1656	1634	0.71	8.48	7.29

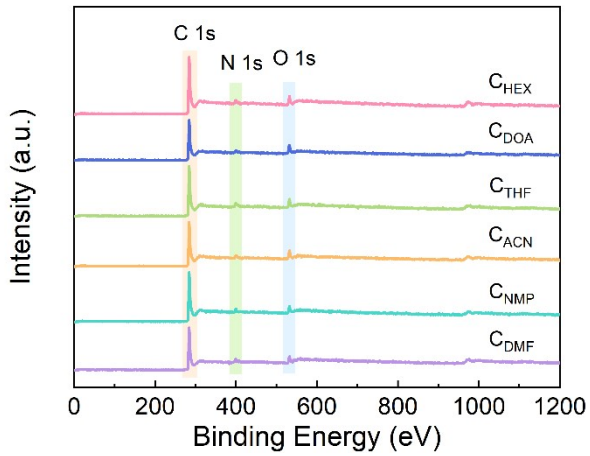

Fig. S3 XPS spectra of C_X.

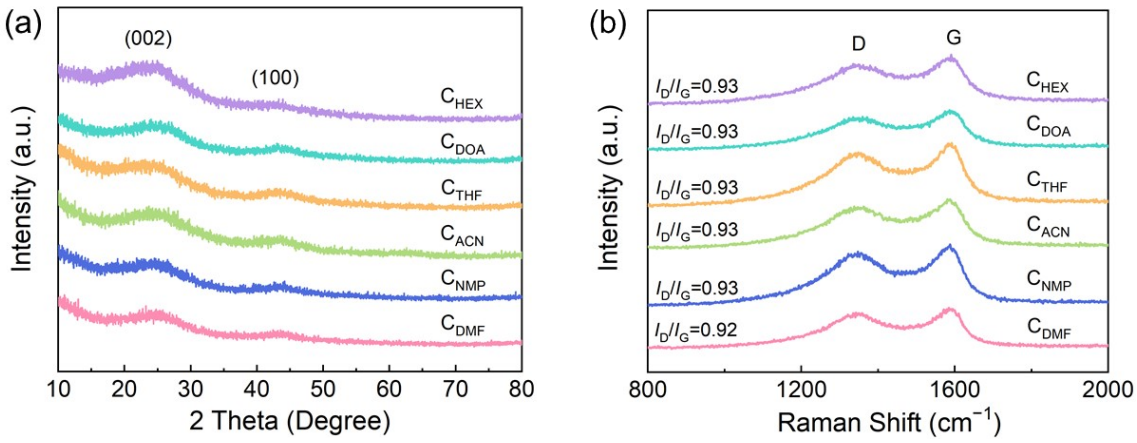

Fig. S4 XRD pattern and Raman spectra of C_X.

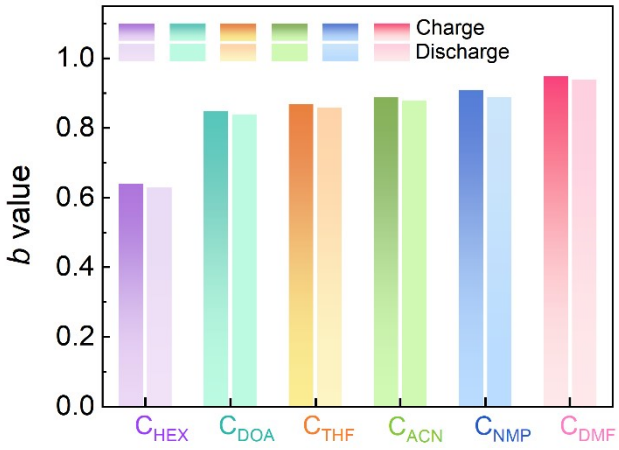

Fig. S5 The *b* values of C_X-based devices in the anodic and cathodic scans from 5 to 500 mV s^{-1}.

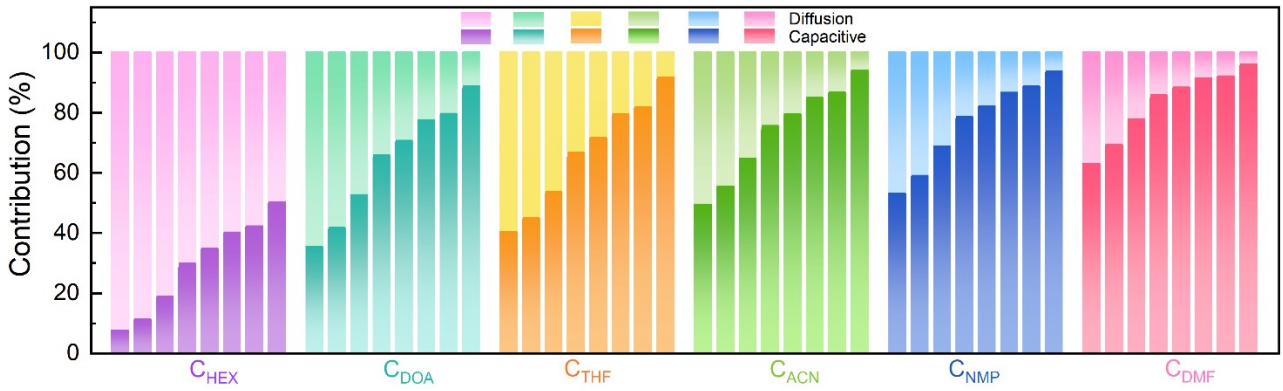

Fig. S6 Capacitive and diffusion-controlled contribution ratios of C_X-based devices at 5, 10, 50, 100, 200, 300, 400, and 500 mV s^{-1}.

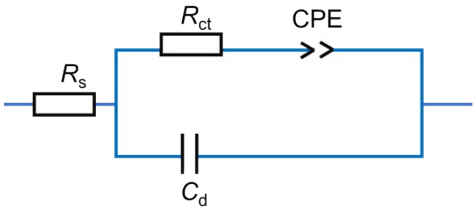

Fig. S7 The equivalent circuit of Nyquist plots. (R_s: internal resistance of the electrode, R_{ct}: charge transfer resistance, CPE*:* constant phase angle element, C_d: electrical double layer capacitor).

Table S3 The comparison of parameters related to charge transfer of C_X.

Device	R_s (Ω)	R_{ct} (Ω)	σ (Ω $s^{-0.5}$)
C_{HEX}	0.65	119.74	201.89
C_{DOA}	0.65	110.68	224.37
C_{THF}	0.99	110.41	185.03
C_{ACN}	0.87	80.34	69.34
C_{NMP}	0.87	11.06	40.61
C_{DMF}	0.63	10.47	17.48

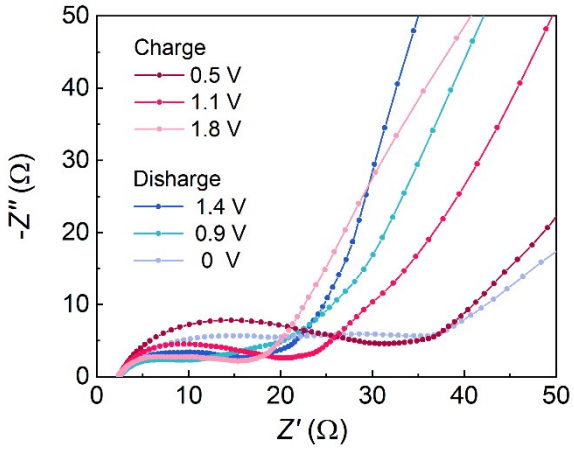

Fig. S8 Nyquist plots of the C_{DMF}-based device measured at different potentials.

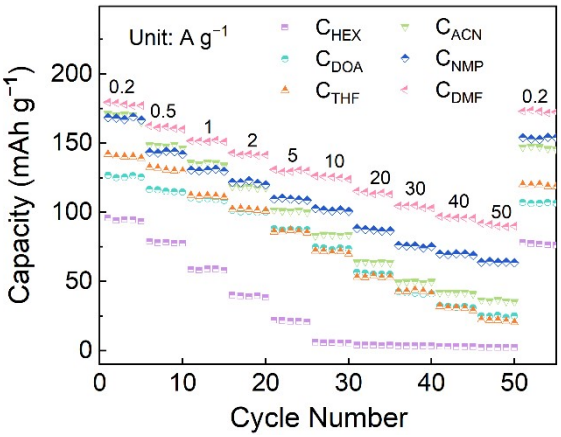

Fig. S9 Capacity reversibility measurements.

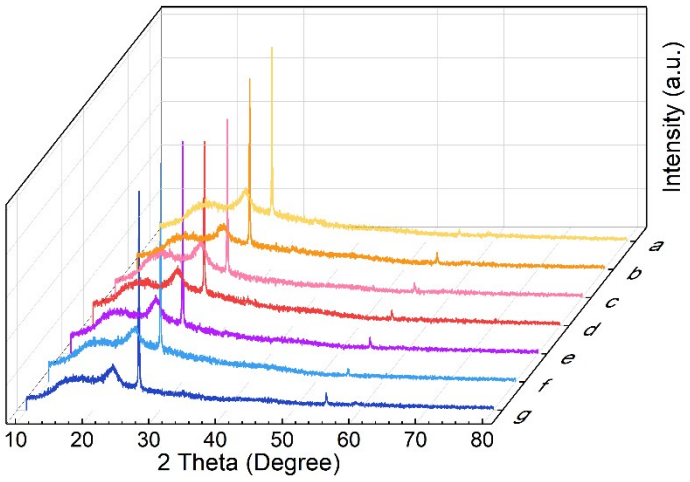

Fig. S10 *Ex situ* XRD patterns of the C_{DMF}-based device during the charging/discharging processes.

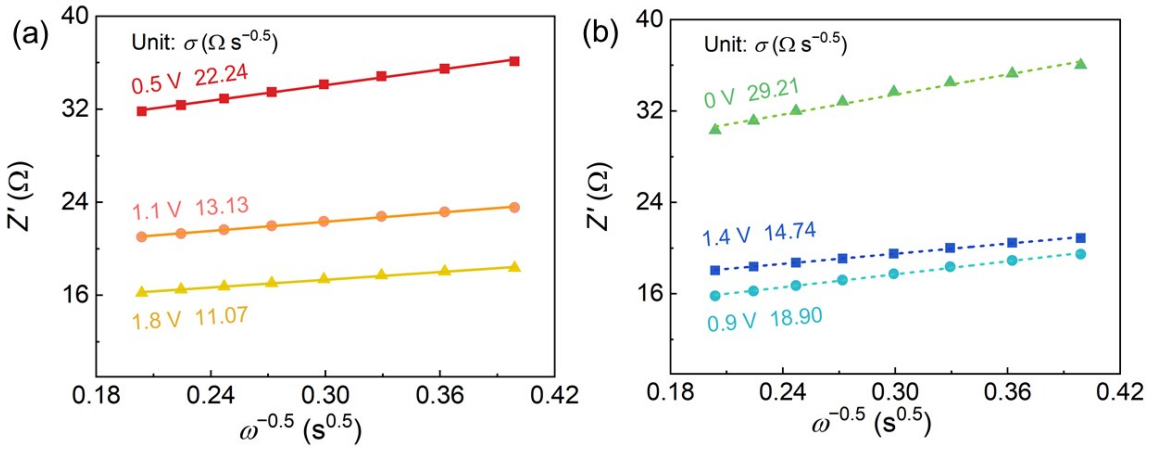

Fig. S11 The linear relation of $\omega^{-0.5}$ versus Z' at (a) charging conditions and (b) discharging conditions.

Table S4 The fitted σ values and $D_{Zn^{2+}}$ of the C_{DMF}-based device at various potentials.

discharge charge

Potential (V)	σ (Ω s$^{-0.5}$)	$D_{Zn^{2+}} \times 10^{-18}$ (cm^2 s^{-1})
0.5	22.24	3.25
1.1	13.13	9.33
1.8	11.07	13.10
1.4	14.74	7.40
0.9	18.90	4.50
0	29.21	1.89

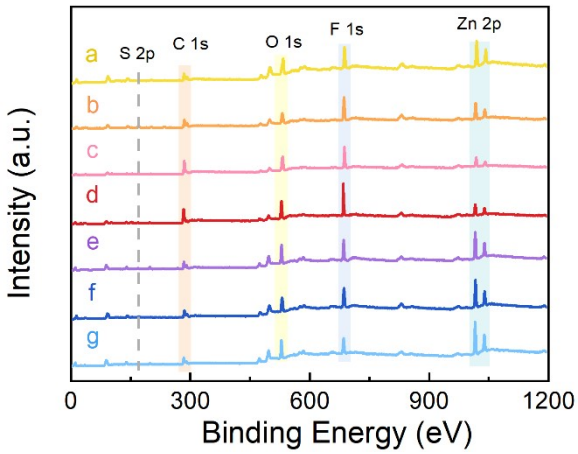

Fig. S12 *Ex situ* XPS spectra at various charging/discharging processes of C_{DMF} device.

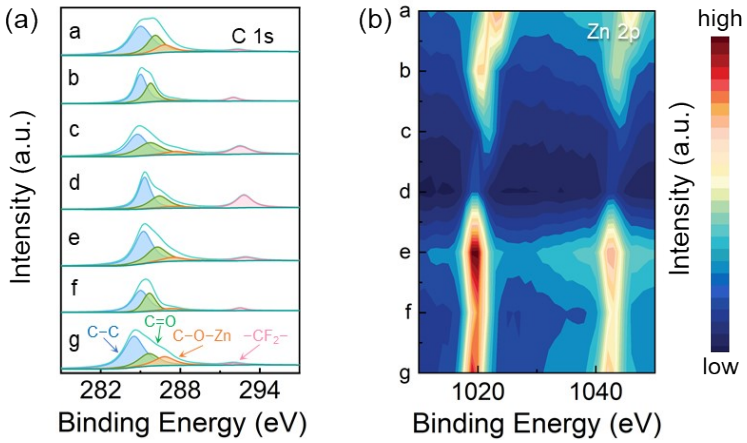

Fig. S13 (a) The C 1s and (b) Zn 2p XPS spectra at various charging/discharging processes of the C_{DMF}-based device.

References

1 H. Launay, C. M. Hansen and K. Almdal, *Carbon*, 2007, **45**, 2859−2865.
2 S. Chen, D. M. Koshy, Y. Tsao, R. Pfattner, X. Yan, D. Feng and Z. Bao, *J. Am. Chem. Soc.*, 2018, **140**, 10297−10304.
3 J. Chen, W. Yan, E. J. Townsend, J. Feng, L. Pan, V. Del Angel Hernandez and C. F. J. Faul, *Angew. Chem. Int. Ed.*, 2019, **58**, 11715−11719.